bioRxiv preprint doi: https://doi.org/10.1101/626457; this version posted May 3, 2019. The copyright holder for this preprint (which was not certified by peer review) is the author/funder, who has granted bioRxiv a license to display the preprint in perpetuity. It is made available under aCC-BY-ND 4.0 International license.

Title

RNA polymerase mutations cause cephalosporin resistance in clinical *Neisseria gonorrhoeae* isolates

Authors

Samantha G. Palace[1,2], Yi Wang[1], Daniel H. F. Rubin[1], Michael A. Welsh[3], Suzanne Walker[3], Yonatan H. Grad[1,2,4]*

Affiliations

[1] Department of Immunology and Infectious Diseases, Harvard T. H. Chan School of Public Health, Boston, MA, USA

[2] Center for Communicable Disease Dynamics, Harvard T. H. Chan School of Public Health, Boston, MA, USA

[3] Department of Microbiology, Harvard Medical School, Boston, MA, USA

[4] Division of Infectious Diseases, Brigham and Women's Hospital, Harvard Medical School, Boston, MA, USA

bioRxiv preprint doi: https://doi.org/10.1101/626457; this version posted May 3, 2019. The copyright holder for this preprint (which was not certified by peer review) is the author/funder, who has granted bioRxiv a license to display the preprint in perpetuity. It is made available under aCC-BY-ND 4.0 International license.

Abstract

The rising incidence of *Neisseria gonorrhoeae* infection and antimicrobial resistance imperils effective therapy for gonococcal infections [1-4]. Current first-line therapy for gonorrhea relies on ceftriaxone (CRO), an extended spectrum cephalosporin (ESC), as the backbone of treatment. Dual therapy with azithromycin was intended to delay the emergence of resistance, but rising azithromycin resistance rates have been reported [2,5], resulting in revision of United Kingdom treatment guidelines to CRO monotherapy [6]. With no clear next-line agent, gonococcal resistance to ESCs is a problem of paramount clinical importance, underscored by recent reports of treatment failure and global spread of a multidrug-resistant strain [4,7]. Reduced susceptibility to ceftriaxone (CRO^{RS}) is most commonly associated with interspecies mosaic and other alleles of *penA* (PBP2) [8-10], the primary target of ESCs [8,11]. However, collections of clinical specimens often include isolates with high-level reduced susceptibility to ESCs (ESC^{RS}) that is not attributable to *penA* variation [3,12,13]. Here, we describe the genetic basis of reduced susceptibility in three such isolates collected in the United States. Each of these isolates has a unique mutation in the RNA polymerase holoenzyme that causes phenotypic CRO^{RS} when introduced into susceptible strains. We demonstrate that other clinical isolates can develop high-level ESC^{RS} via a single nucleotide change in RNA polymerase. This result has important implications regarding the biology underlying cephalosporin resistance, the potential for *de novo* evolution of resistance under cephalosporin monotherapy, and the accuracy of sequence-based diagnostics.

Introduction

A recent report [14] described a clinical gonococcal isolate, GCGS1095, with a cefixime (CFX) minimum inhibitory concentration (MIC) of 1 µg/mL and a CRO MIC of 0.5 µg/mL, well above the Center for Disease Control and Prevention's Gonococcal Isolate Surveillance Project

bioRxiv preprint doi: https://doi.org/10.1101/626457; this version posted May 3, 2019. The copyright holder for this preprint (which was not certified by peer review) is the author/funder, who has granted bioRxiv a license to display the preprint in perpetuity. It is made available under aCC-BY-ND 4.0 International license.

(GISP) definitions for CFX^{RS} (0.25µg/mL) and CRO^{RS} (0.125 µg/mL) [2]. The type II non-mosaic *penA* allele found in this isolate is not known to contribute to reduced cephalosporin susceptibility and is found in many ESC susceptible isolates [15]. While other loci are known to contribute to ESC^{RS}, including mutations in *porB* that affect drug permeability, mutations that enhance drug efflux through the MtrCDE pump, and mutations in penicillin-binding proteins [9,10], the genotype of GCGS1095 at these loci does not explain its high-level CRO^{RS} phenotype [14]. GCGS1014, a second clinical isolate from the same GISP collection, also has an unexplained CRO^{RS} phenotype (Table 1). The close phylogenetic relationship between GCGS1095 and GCGS1014 (Figure 1A) suggests that they likely share the same unknown genetic basis of reduced ESC susceptibility, which we sought to identify.

Results and Discussion

The two CRO^{RS} isolates GCGS1095 and GCGS1014 are phylogenetically interleaved with two ceftriaxone-susceptible (CRO^{S}) isolates (GCGS0335 and GCGS0324; CRO MIC 0.008 and 0.015 µg/mL, respectively). The phenotypic distinction among these closely related CRO^{S} and CRO^{RS} isolates led us to postulate that the unknown genetic determinant of CRO^{RS} in GCGS1095 and GCGS1014 would be absent in both susceptible isolates. However, a genomic comparison of single nucleotide variants failed to identify any variants that were exclusively present in both CRO^{RS} isolates.

To identify the genetic basis of reduced susceptibility in GCGS1095 and GCGS1014, we took an experimental approach that leveraged the natural transformability of gonococcus. Genomic DNA from each CRO^{RS} isolate was used to transform a susceptible recipient strain. Transformants that acquired the CRO^{RS} phenotype were characterized by whole genome sequencing to define the transformed loci. Repeated attempts to transform the laboratory strain

bioRxiv preprint doi: https://doi.org/10.1101/626457; this version posted May 3, 2019. The copyright holder for this preprint (which was not certified by peer review) is the author/funder, who has granted bioRxiv a license to display the preprint in perpetuity. It is made available under aCC-BY-ND 4.0 International license.

28BL to CRO^{RS} using genomic DNA from GCGS1095 or GCGS1014 were unsuccessful, despite successful transformation of this strain using other DNA (including genomic DNA from an isolate with a CRO^{RS}-associated mosaic *penA* allele). By contrast, transformation of genomic DNA from either of these CRO^{RS} isolates into the susceptible recipient isolate GCGS0457 (CRO MIC 0.016 μg/mL) – a phylogenetic neighbor of GCGS1095 and GCGS1014 (Figure 1A) – yielded multiple CRO^{RS} transformants, indicating that genetic background constrained the acquisition or expression of reduced susceptibility.

All CRO^{RS} transformants from GCGS1095 gDNA inherited a single nucleotide polymorphism (SNP) in *rpoB* (nucleotide change G602A), which encodes the RNA polymerase beta subunit RpoB (amino acid substitution RpoB^{R201H}). CRO^{RS} transformants from GCGS1014 gDNA inherited a single nucleotide substitution in *rpoD* (nucleotide G292A), which encodes the major housekeeping sigma factor RpoD (amino acid substitution RpoD^{E98K}). Each of these variants was present only in the corresponding donor strain (RpoB^{R201H} in GCGS1095 and RpoD^{E98K} in GCGS1014), but not in both CRO^{RS} isolates (Table 1, Figure 1B). The identification of two distinct mutations in different components of the RNA polymerase holoenzyme explains the failure of our comparative genomic approach to identify a single variant shared exclusively between GCGS1095 and GCGS1014.

To validate these candidate polymorphisms, GCGS0457 was transformed with PCR-amplified DNA segments from GCGS1095 and GCGS1014 that include ~1.5kb of flanking homology around the *rpoB* G602A or the *rpoD* G292A variant positions. With the exception of SNPs of interest, each PCR product is identical to the recipient (GCGS0457) sequence. Transformation with *rpoB*^{GCGS1095} or *rpoD*^{GCGS1014} PCR products yielded multiple CRO^{RS} transformants, whereas transformation with the control PCR products *rpoB*^{GCGS1014} and

bioRxiv preprint doi: https://doi.org/10.1101/626457; this version posted May 3, 2019. The copyright holder for this preprint (which was not certified by peer review) is the author/funder, who has granted bioRxiv a license to display the preprint in perpetuity. It is made available under aCC-BY-ND 4.0 International license.

rpoD^{GCGS1095} yielded none. Sanger sequencing confirmed the presence of the expected SNP in each resistant transformant. Representative CRO^{RS} transformants were further examined by whole genome sequencing, which ruled out spontaneous mutations. The *rpoB*^{GCGS1095} and *rpoD*^{GCGS1014} transformants GCGS0457 RpoB^{R201H} and GCGS0457 RpoD^{E98K} (respectively) had CRO MICs similar to the parental CRO^{RS} isolates (Table 1), indicating that each of these SNPs is sufficient to fully recapitulate the CRO^{RS} phenotype in the GCGS0457 background.

As GCGS1095 and GCGS1014 have distinct RNA polymerase (RNAP) mutations, we hypothesized that additional RNAP variants might explain other cases of uncharacterized CRO^{RS}. We found one additional *rpoD* allele in the GISP strain collection that has this effect: a 12-basepair in-frame internal deletion in *rpoD*, resulting in the deletion of amino acids 92-95. This allele is uniquely found in the CRO^{RS} isolate GCGS1013 (CRO MIC 0.125 μg/mL; no CRO^{RS}-associated *penA* allele; Table 1). Transformation of the *rpoD*^{GCGS1013} allele into the susceptible isolate GCGS0457 increased CRO resistance to 0.125 μg/mL (Table 1). The amino acids deleted in the RpoD$^{\Delta 92\text{-}95}$ allele of GCGS1013 are in a similar region of the RpoD protein as the single amino acid change in the GCGS1014 allele RpoD^{E98K} (Figure 1B), despite the phylogenetic separation of these isolates (Figure 1A). Taken together, these results demonstrate that RNAP-mediated CRO^{RS} has arisen multiple times in clinical isolates of *N. gonorrhoeae*.

The identification of the *rpoB* and *rpoD* SNPs in GCGS1095 and GCGS1014 indicates that other gonococcal isolates may be a single mutation from high-level CRO^{RS}. However, given the apparent incompatibility of this resistance mechanism with the 28BL strain, the development of CRO^{RS} via this pathway may require one or more genetic background factors that are yet to be defined. It is therefore not immediately apparent which circulating strains might acquire this resistance mechanism. In preliminary studies using genetically diverse CRO^{S} isolates as recipient

bioRxiv preprint doi: https://doi.org/10.1101/626457; this version posted May 3, 2019. The copyright holder for this preprint (which was not certified by peer review) is the author/funder, who has granted bioRxiv a license to display the preprint in perpetuity. It is made available under aCC-BY-ND 4.0 International license.

strains for transformation, we found five additional isolates dispersed throughout the phylogeny that are able to acquire phenotypic CRO^{RS} following transformation with the GCGS1095 *rpoB* allele ($RpoB^{R201H}$), indicating that genetic background compatibility with this resistance mechanism is not limited to a single gonococcal lineage (Figure 1A) or to genetic backgrounds with particular genotypes of various RNA polymerase components (Supplementary File 1). Furthermore, we found that the CRO^{S} isolate GCGS0364 spontaneously developed CRO^{RS} *in vitro* via *rpoB* mutations (Figure 1A-B). These *de novo* mutations are predicted to occur in a region of the RpoB protein very close to the $RpoB^{R201H}$ variant position found in GCGS1095 (Figure 1C). As with the other RNAP mutations we tested, targeted transformation of these spontaneous mutations from GCGS0364 into a susceptible background caused high-level phenotypic CRO^{RS} (Table 1).

It is not known how RNAP mutations reduce susceptibility to ESCs, a class of cell wall biosynthesis inhibitors. To address this question, we examined whether these RNAP mutations cause a slow-growth or general stress response phenotype that increases resistance to diverse classes of antimicrobial compounds. We found that introduction of the CRO^{RS}-associated alleles $RpoB^{R201H}$, $RpoD^{E98K}$, or $RpoD^{\Delta 92\text{-}95}$ into the CRO^{S} strain GCGS0457 conferred reduced susceptibility to the third-generation cephalosporins CRO and CFX, but did not affect susceptibility to antimicrobial drugs that do not target the cell wall, including ciprofloxacin, tetracycline, azithromycin, and rifampicin. Surprisingly, these mutations also failed to confer resistance to the non-cephalosporin β-lactams penicillin and ertapenem (Figure 2A). GCGS0457 $RpoB^{R201H}$ and GCGS0457 $RpoD^{E98K}$ transformants did not have a significant growth defect *in vitro* when grown on the rich medium used for antimicrobial susceptibility testing (Figure 2B), and CRO^{RS} transformants had no gross defects in cell morphology by transmission electron

bioRxiv preprint doi: https://doi.org/10.1101/626457; this version posted May 3, 2019. The copyright holder for this preprint (which was not certified by peer review) is the author/funder, who has granted bioRxiv a license to display the preprint in perpetuity. It is made available under aCC-BY-ND 4.0 International license.

microscopy (TEM) (Figure 2C), although transformants were slightly smaller than the parental GCGS0457 strain (Supplementary Figure 1).

The observation that the RNAP mutations identified here do not broadly change antimicrobial susceptibility profiles or growth phenotypes supports the hypothesis that these mutations generate a cephalosporin-specific resistance mechanism, as opposed to a large-scale physiological shift toward a generally antibiotic-tolerant state. Altered activity of the RNA polymerase transcription machinery could result in this type of drug-specific reduced susceptibility, particularly if these RNAP variants differentially express one or more transcripts relating to the cephalosporin mode of action. We used RNA-seq to examine the transcriptional profiles of the CRO^{RS} isolates GCGS1095 and GCGS1014 and the susceptible isolate GCGS0457. The transcriptional profiles of the CRO^{RS} isolates were similar to one another but distinct from GCGS0457 (Supplementary Figure 2), with 1337 and 1410 annotated ORFs significantly altered in abundance, respectively. The transcriptomic differences we observe may partly reflect the genetic distance between these isolates [16], as the resistant strains GCGS1095 and GCGS1014 are more closely related to one another than they are to GCGS0457. We therefore compared GCGS0457 to its isogenic CRO^{RS} transformants GCGS0457 $RpoB^{R201H}$ and GCGS0457 $RpoD^{E98K}$. The $RpoB^{R201H}$ and $RpoD^{E98K}$ alleles each profoundly altered the transcriptional profile of GCGS0457: 1278 annotated ORFs in the $RpoD^{E98K}$ transformant and 1218 annotated ORFs in the $RpoB^{R201H}$ transformant were differentially expressed relative to the parental GCGS0457 strain. The transcriptional profiles of the two transformants were very similar to one another (Supplementary Figure 2), indicating that these different mutations have similar functional consequences. Overall, a total of 890 annotated ORFs were differentially expressed in all four CRO^{RS} strains (CRO^{RS} isolates and isogenic transformants) compared to

bioRxiv preprint doi: https://doi.org/10.1101/626457; this version posted May 3, 2019. The copyright holder for this preprint (which was not certified by peer review) is the author/funder, who has granted bioRxiv a license to display the preprint in perpetuity. It is made available under aCC-BY-ND 4.0 International license.

GCGS0457. The vast majority of the transcriptional changes are small in magnitude (90%, or 805/890, are less than 2-fold differentially expressed in one or more of the CRO^{RS} strains), perhaps explaining the apparent lack of a major fitness defect in these strains.

Altered expression of resistance-associated genes such as efflux pumps and β-lactamases is a common mechanism of transcriptionally-mediated drug resistance. Although these strains lack a TEM-1 β-lactamase [12], increased expression of the gonococcal MtrCDE efflux pump is known to increase resistance to β-lactams, including cephalosporins. [9] However, transcription of the operon encoding this pump is not elevated in the CRO^{RS} RNAP mutants (Supplementary Figure 3), nor is it differentially upregulated in response to drug exposure in these strains (Supplementary Figure 4). Since ESCs, like other β-lactams, block cell wall biosynthesis by covalently inhibiting penicillin-binding proteins (PBPs), we examined how CRO^{RS}-associated RNAP mutations affect expression of enzymes in this target pathway. *N. gonorrhoeae* encodes four known PBPs [17,18]: the essential high-molecular weight bifunctional transpeptidase/transglycosylase PBP1 (encoded by *ponA*); the essential high-molecular weight transpeptidase PBP2 (encoded by *penA*), which is the primary target of ESCs [8,11]; and the nonessential carboxypeptidases PBP3 (encoded by *dacB*) and PBP4 (encoded by *pbpG*), as well as DacC (encoded by *dacC*), a third putative low-molecular weight carboxypeptidase that lacks conserved active site motifs [18]. A homologue of the L,D-transpeptidase YnhG is also present in the genome, although it has not been reported to be functional in *N. gonorrhoeae*. CRO^{RS}-associated RNAP mutations did not increase mRNA or protein abundance of the CRO target PBP2 (Figure 3). Transcription of the putative L,D-transpeptidase gene *ynhG* was not altered in the CRO^{RS} strains (Supplementary Figure 3). However, PBP1 (*ponA*) is upregulated in each of the CRO^{RS} strains compared to GCGS0457, while expression of PBP3, *pbpG*, and *dacC* is

bioRxiv preprint doi: https://doi.org/10.1101/626457; this version posted May 3, 2019. The copyright holder for this preprint (which was not certified by peer review) is the author/funder, who has granted bioRxiv a license to display the preprint in perpetuity. It is made available under aCC-BY-ND 4.0 International license.

decreased in these strains (Figure 3A-B). Similar expression patterns were observed in the presence of sub-inhibitory CRO (Supplementary Figure 4). These altered PBP expression patterns are reflected in the cell wall structure of the CRO^{RS} strains: reduced expression of the carboxypeptidases results in more peptidoglycan with pentapeptide stems (Figure 3C, Supplementary Figure 5, and Supplementary Table 2), in agreement with reported structural changes of cell walls from strains lacking the DacB carboxypeptidase [18]. The increased expression of PBP1 in these RNAP mutants does not appear to increase the abundance of crosslinked peptidoglycan (Supplementary Figure 5 and Supplementary Table 2).

Although PBP1 and PBP2 both catalyze transpeptidation, PBP1 is not efficiently inhibited by third-generation cephalosporins [11]. We therefore tested whether increased PBP1 expression could cause the CRO^{RS} phenotype, potentially via compensating for the reduced PBP2-mediated transpeptidation during drug treatment. We introduced a second copy of the *ponA* (PBP1) gene under control of the lac promoter into the GCGS0457 strain using the pKH37 complementation system [19]. Overexpression of *ponA* from this locus increased CRO MIC from 0.016 μg/mL to 0.064 μg/mL (Table 1). Expression of the $PBP1^{L421P}$ variant that has previously been associated with β-lactam resistance [9,20] did not further increase CRO MIC in this overexpression assay (Table 1).

While increasing the PBP1 expression level contributes to phenotypic CRO^{RS}, therefore, PBP1 overexpression in the GCGS0457 background is not sufficient to fully recapitulate the high-level CRO^{RS} phenotype (MIC ≥ 0.125 μg/mL) observed in strains with RNAP mutations. *In vitro* evolution studies that evolve cephalosporin resistance in *N. gonorrhoeae* identified inactivating mutations in the type IV pilus pore subunit PilQ [21,22], although similar *pilQ* mutations have not been identified in clinical isolates, presumably because colonization requires

bioRxiv preprint doi: https://doi.org/10.1101/626457; this version posted May 3, 2019. The copyright holder for this preprint (which was not certified by peer review) is the author/funder, who has granted bioRxiv a license to display the preprint in perpetuity. It is made available under aCC-BY-ND 4.0 International license.

pilus-mediated adhesion to epithelial cells [23,24]. Notably, *pilQ* transcription is reduced in RpoB^{R201H} and RpoD^{E98K} transformants and in the CRO^{RS} isolates GCGS1095 and GCGS1014 (Supplementary Figure 3 and 4), suggesting hypomorphic *pilQ* expression may contribute to reducing cephalosporin susceptibility without eliminating pilus-mediated attachment and colonization altogether. The pleiotropy of RNAP mutations, resulting in simultaneous alteration of multiple transcript abundances, may thus enable a multicomponent resistance mechanism to emerge following a single genetic change.

We have demonstrated that these RNAP mutations cause high-level ESC^{RS} in multiple clinical isolates. The identification of three independent mutations in two separate components of the RNA polymerase machinery illustrates challenges faced by computational genomic analytical strategies to describe new resistance alleles. Continued isolate collection, phenotypic characterization, and traditional genetic techniques will be critical for defining emerging resistance mechanisms. The observation that multiple lineages can gain CRO resistance through RNAP mutations further underscores the need to monitor for the development of CRO^{RS} through pathways other than *penA* mutations, particularly as the ESCs are increasingly relied upon for treatment. Identifying these alternative genetic mechanisms of reduced susceptibility is needed to support the development of accurate and reliable sequence-based diagnostics that predict CRO susceptibility as well as to aid in the design of novel therapeutics.

Methods

Bacterial strains and culture conditions. Strains are presented in Supplementary Table 1. Except where otherwise specified, *N. gonorrhoeae* was cultured on GCB agar (Difco) with Kellogg's supplements (GCB-K) [23] at 37°C in a 5% CO_2 atmosphere. Antibiotic susceptibility

bioRxiv preprint doi: https://doi.org/10.1101/626457; this version posted May 3, 2019. The copyright holder for this preprint (which was not certified by peer review) is the author/funder, who has granted bioRxiv a license to display the preprint in perpetuity. It is made available under aCC-BY-ND 4.0 International license.

testing of *N. gonorrhoeae* strains was performed on GCB media supplemented with 1% IsoVitaleX (Becton Dickinson) via agar dilution or Etest (bioMérieux). *E. coli* strains were cultured in LB medium at 37°C. Media were supplemented as appropriate with chloramphenicol (20 μg/mL for *E. coli*; 1 μg/mL for *N. gonorrhoeae*).

Transformation of reduced cephalosporin susceptibility with genomic DNA. CRO^S recipient strains GCGS0457 and 28BL were transformed with genomic DNA from GCGS1014 and GCGS1095. Transformations were conducted in liquid culture as described [25,26]. Briefly, piliated *N. gonorrhoeae* was suspended in GCP medium (15 g/L protease peptone 3, 1 g/L soluble starch, 4 g/L dibasic K_2HPO_4, 1 g/L monobasic KH_2PO_4, 5 g/L NaCl) with Kellogg's supplement, 10mM $MgCl_2$, and approximately 100 ng genomic DNA. Suspensions were incubated for 10 minutes at 37°C with 5% CO_2. Transformants were allowed to recover on nonselective agar for 4-5 hours. After recovery, transformants were plated on GCB-K ceftriaxone gradient agar plates, which were prepared by allowing a 40 μL droplet of 5 μg/mL ceftriaxone to dry onto a GCB-K agar plate. Transformations performed with GCGS0457 genomic DNA served as controls to monitor for spontaneous CRO^{RS} mutation. After outgrowth at 37°C in 5% CO_2, colonies growing within the ceftriaxone zone of inhibition were subcultured for further analysis.

Transformation of RNA polymerase mutations. ~1.5kb PCR fragments surrounding the *rpoB* and *rpoD* loci of interest were amplified using the primer pairs RpoB-US (5'-<u>ATGCCGTCTGAA</u>TATCAGATTGATGCGTACCGTT-3') and RpoB-DS (5'-CGTACTCGACGGTTGCCCAAG-3') or RpoD-US (5'-AACTGCTCGGACAGGAAGCG-3') and RpoD-DS (5'-CGCGTTCGAGTTTGCGGATGTT-3'). The 12-bp DNA uptake sequence (DUS) for *N. gonorrhoeae* [27] was added to the 5' end of the RpoB-US primer (underlined) to enhance transformation efficiency with the PCR product; a DUS was not added to the RpoD-US

bioRxiv preprint doi: https://doi.org/10.1101/626457; this version posted May 3, 2019. The copyright holder for this preprint (which was not certified by peer review) is the author/funder, who has granted bioRxiv a license to display the preprint in perpetuity. It is made available under aCC-BY-ND 4.0 International license.

or RpoD-DS primers, as the PCR product amplified by these primers includes two endogenous DUS regions. CRO^S recipient strains were transformed with 200-300 ng purified PCR products and transformants were selected for CRO^{RS} as above. Transformation reactions performed with wildtype alleles (*rpoB* from GCGS1014; *rpoD* from GCGS1095) served as controls to monitor for spontaneous CRO^{RS} mutation.

Sequencing and analysis. Following undirected transformation of GCGS0457 with GCGS1014 or GCGS1095 genomic DNA, or directed transformation of GCGS0457 with PCR products, CRO^{RS} transformants were analyzed by whole genome sequencing. Genomic DNA of transformants was purified with the PureLink Genomic DNA Mini kit (Life Technologies) and sequencing libraries were prepared as described [28]. Paired-end sequencing of these libraries was performed on an Illumina MiniSeq (Illumina). Reads were aligned to the *de novo* assembly of the GCGS0457 genome (European Nucleotide Archive, accession number ERR855051) using bwa v0.7.8 [29], and variant calling was performed with pilon v1.22 [30]. For each isolate in the GISP collection, the sequence of RNA polymerase components was identified using BLASTn (ncbi-blast v2.2.30) (Supplemental File 1).

Growth curves. Bacterial cells grown overnight on GCB-K plates were suspended in tryptic soy broth to OD_{600} 0.01. Three replicate GCB-K plates per time point were inoculated with 0.1 mL of this suspension and incubated at 37°C with 5% CO_2. At each time point, the lawn of bacterial growth from each of three replicate plates was suspended in tryptic soy broth. Serial dilutions were plated on GCB-K to determine total CFUs per plate. CFU counts were normalized to the initial inoculum density (CFUs measured at time 0) for each replicate.

Transmission electron microscopy. Bacterial cells grown overnight on GCB-K plates were suspended in liquid GCP medium with 1% Kellogg's supplement and 0.042% $NaHCO_3$ to OD_{600}

bioRxiv preprint doi: https://doi.org/10.1101/626457; this version posted May 3, 2019. The copyright holder for this preprint (which was not certified by peer review) is the author/funder, who has granted bioRxiv a license to display the preprint in perpetuity. It is made available under aCC-BY-ND 4.0 International license.

0.1. Suspensions were incubated at 37°C with aeration for 2 hours to allow cultures to return to log phase. Cell pellets were collected by centrifugation and fixed for at least two hours at room temperature in 0.2M cacodylate buffer with 2.5% paraformaldehyde, 5% glutaraldehyde, and 0.06% picric acid. Fixed pellets were washed in 0.1M cacodylate buffer and postfixed with 1% Osmiumtetroxide (OsO4)/1.5% Potassiumferrocyanide (KFeCN6) for 1 hour, washed 2x in water, 1x Maleate buffer (MB) 1x and incubated in 1% uranyl acetate in MB for 1hr followed by 2 washes in water and subsequent dehydration in grades of alcohol (10min each; 50%, 70%, 90%, 2x10min 100%). The samples were then put in propyleneoxide for 1 hr and infiltrated ON in a 1:1 mixture of propyleneoxide and TAAB Epon (Marivac Canada Inc. St. Laurent, Canada). The following day the samples were embedded in TAAB Epon and polymerized at 60 degrees C for 48 hrs. Ultrathin sections (~60nm) were cut on a Reichert Ultracut-S microtome, picked up on to copper grids stained with lead citrate and examined in a JEOL 1200EX Transmission electron microscope or a TecnaiG² Spirit BioTWIN and images were recorded with an AMT 2k CCD camera.

Transcriptomics. RNA isolation and sequencing was performed from *N. gonorrhoeae* strains as described [26]. Bacterial cells grown on GCB-K plates for 17 hours were suspended in liquid GCP medium with 1% IsoVitaleX and 0.042% $NaHCO_3$ to OD_{600} 0.1. Suspensions were incubated at 37°C with aeration for 2-3 hours to allow cultures to return to log phase. Cells were collected to measure baseline transcriptional profiles (shown in Figure 3 and Supplementary Figure 3). For samples that measured the effect of drug exposure (Supplementary Figure 4), 0.008 μg/mL (sub-inhibitory) CRO was added and cultures were incubated at 37°C for an additional 90 minutes before cell collection. RNA was purified with the Direct-Zol kit (Zymo). Transcriptome libraries were prepared at the Broad Institute at the Microbial 'Omics Core using a modified version of

bioRxiv preprint doi: https://doi.org/10.1101/626457; this version posted May 3, 2019. The copyright holder for this preprint (which was not certified by peer review) is the author/funder, who has granted bioRxiv a license to display the preprint in perpetuity. It is made available under aCC-BY-ND 4.0 International license.

the RNAtag-seq protocol [31]. Five hundred nanograms of total RNA was fragmented, depleted of genomic DNA, dephosphorylated, and ligated to DNA adapters carrying 5'-AN8-3' barcodes of known sequence with a 5' phosphate and a 3' blocking group. Barcoded RNAs were pooled and depleted of rRNA using the RiboZero rRNA depletion kit (Epicentre). Pools of barcoded RNAs were converted to Illumina cDNA libraries in two steps: (i) reverse transcription of the RNA using a primer designed to the constant region of the barcoded adapter with addition of an adapter to the 3' end of the cDNA by template switching using SMARTScribe (Clontech) as described previously [32]; (ii) PCR amplification using primers whose 5' ends target the constant regions of the 3' or 5' adapter and whose 3' ends contain the full Illumina P5 or P7 sequences. cDNA libraries were sequenced on the Illumina Nextseq 500 platform to generate 50-bp paired-end reads. Barcode sequences were removed, and reads were aligned to the FA1090 reference genome. Read counts were assigned to genes and other genomic features using custom scripts. Differential expression analysis was conducted in DESeq2 v.1.16.1 [33].

Sequence data availability. Genomic and transcriptomic read libraries are available from the NCBI SRA database (accession number PRJNA540288).

PBP abundance measurement. Protein abundance of PBP1, PBP2, and PBP3 was calculated using the fluorescent penicillin derivative bocillin-FL (Thermo Fisher). *N. gonorrhoeae* strains from overnight cultures were suspended in liquid GCP medium supplemented with 1% IsoVitalex and 0.042% $NaHCO_3$ to a density of OD_{600} 0.1. Suspensions were incubated with aeration at 37°C for 2.5-3 hours. Bacterial cells were collected by centrifugation, washed once with 1 mL of sterile phosphate-buffered saline (PBS), and resuspended in PBS 5 μg/mL bocillin-FL and 0.1% dimethyl sulfoxide (DMSO) to a final concentration of 1 mL of OD_{600} 0.5 per 50 μL suspension. Bocillin-FL suspensions were incubated for 5 minutes. An equal volume 2x

bioRxiv preprint doi: https://doi.org/10.1101/626457; this version posted May 3, 2019. The copyright holder for this preprint (which was not certified by peer review) is the author/funder, who has granted bioRxiv a license to display the preprint in perpetuity. It is made available under aCC-BY-ND 4.0 International license.

SDS-PAGE sample buffer (Novex) was added and samples were boiled for 5 minutes. Proteins in 30 μL of each suspension were separated by SDS-PAGE on 4-12% Tris-Glycine protein gels (Novex), which were visualized on a Typhoon imager (Amersham) (excitation 488 nm/emission 526 nm) to detect bocillin-FL fluorescence. Densitometry was performed with ImageJ [34]. Total bocillin-FL fluorescent signal was calculated for each sample, and the proportional contribution of individual PBPs to this signal was reported.

Muropeptide analysis. *N. gonorrhoeae* strains were cultured for approximately 18 hours at 37°C with agitation in GCP medium supplemented with Kellogg's reagent and 0.042% $NaHCO_3$. Peptidoglycan was isolated and digested as described [35] with minor modifications. Briefly, bacterial cells were pelleted by centrifugation, suspended in 1 mL 1M NaCl, and incubated at 100°C for 20 minutes. Samples were centrifuged for one minute at 18,000×*g*. Pellets were washed three times with water, suspended in 1 mL water, and placed in a bath sonicator for 30 minutes. 0.5 mL 0.1M Tris pH 6.8, 40 μg/mL RNase, and 16 μg/mL DNase were added to each sample; samples were incubated with shaking at 37°C for two hours, with the addition of 16 μg/mL trypsin after the first hour of incubation. Samples were heated to 100°C for 5 minutes to inactivate enzymes, then centrifuged for 3 minutes at 18,000×*g* to pellet peptidoglycan. Pellets were washed with 1 mL aliquots of water until the suspension pH measured between 5 and 5.5. Peptidoglycan was then resuspended in 0.2 mL 12.5mM NaH_2PO_4 pH 5.5 with 500 U/mL mutanolysin and incubated with shaking at 37°C for 16 hours. Samples were heated to 100°C for 5 minutes to inactivate mutanolysin and centrifuged for 5 minutes at 18,000×*g* to pellet debris. The supernatant, containing solubilized muropeptides, was removed to new tubes, and 50 μL 10mg/mL $NaBH_4$ was added to each. Samples were incubated at room temperature for 30 minutes and then the pH was adjusted to 2-3 with 85% H_3PO_4.

bioRxiv preprint doi: https://doi.org/10.1101/626457; this version posted May 3, 2019. The copyright holder for this preprint (which was not certified by peer review) is the author/funder, who has granted bioRxiv a license to display the preprint in perpetuity. It is made available under aCC-BY-ND 4.0 International license.

LC-MS was conducted using an Agilent Technologies 1200 series HPLC in line with an Agilent 6520 Q-TOF mass spectrometer operating with electrospray ionization (ESI) and in positive ion mode. The muropeptide fragments were separated on a Waters Symmetry Shield RP18 column (5 µm, 4.6 x 250 mm) using the following method: 0.5 mL/minute solvent A (water, 0.1% formic acid) for 10 minutes followed by a linear gradient of 0% solvent B (acetonitrile, 0.1% formic acid) to 20% B over 90 minutes.

Construction of strains with inducible *ponA* overexpression. The *ponA* gene was amplified with its native promoter from 28BL (wildtype *ponA*) or from GCGS0457 (*ponA* encoding the PBP1^{L421P} allele) and cloned into the pKH37 plasmid [19] between the PacI and PmeI restriction sites, under control of the lac inducible promoter. The primers used to amplify the *ponA* gene were PBP1-US (5'-AACTTAATTAAGATGAAAGTTCCTGCTTT-3') (PacI site underlined) and PBP1-DS (5'-AACGTTTAAACCCTCAATTATACGGAAACC-3') (PmeI site underlined). The empty vector pKH37 and the plasmids containing the desired *ponA* sequences were methylated with HaeIII methyltransferase (New England Biolabs), linearized with the restriction enzyme PciI (New England Biolabs), and transformed into GCGS0457 via spot transformation as described [19,36]. Overexpression of PBP1 protein was confirmed by bocillin-FL measurement of PBP abundance as described above (Supplementary Figure 6).

Acknowledgements.

We thank the Centers for Disease Control and Prevention Gonococcal Isolate Surveillance Program, Joseph Dillard, Steven Johnson, and Caroline Genco for generously providing strains; Georgia Lagoudas and Paul Blainey for sequencing undirected transformants; Jessica Alexander, Jonathan Livny, and the Broad Institute Microbial 'Omics Core for RNAseq

bioRxiv preprint doi: https://doi.org/10.1101/626457; this version posted May 3, 2019. The copyright holder for this preprint (which was not certified by peer review) is the author/funder, who has granted bioRxiv a license to display the preprint in perpetuity. It is made available under aCC-BY-ND 4.0 International license.

support; the Harvard Medical School Electron Microscopy Facility for TEM imaging; and Crista Wadsworth and Mohamad Rustom Abdul Sater for advising on analysis pipelines.

This work was supported by the Richard and Susan Smith Family Foundation (to YHG) and the National Institutes of Health R01 AI132606 (to YHG), R01 GM76710 (to SW), and F32 GM123579 (to MAW).

Author contributions. SGP and YHG designed and coordinated the study. SGP, YW, DHFR, and MAW performed experiments and data analysis. SGP and YHG wrote the manuscript with input from all authors. MAW and SW provided critical manuscript revision. SW and YHG contributed funding, resources, and supervision.

bioRxiv preprint doi: https://doi.org/10.1101/626457; this version posted May 3, 2019. The copyright holder for this preprint (which was not certified by peer review) is the author/funder, who has granted bioRxiv a license to display the preprint in perpetuity. It is made available under aCC-BY-ND 4.0 International license.

Table 1. Selected strains, phenotypic ceftriaxone susceptibility, and relevant genotypes.

strain	CRO MIC (µg/mL)	*penA* (PBP2)	*ponA* (PBP1)	RpoB	RpoD
GCGS0457	0.016	Type II non-mosaic (NG STAR 2.002)	421P	wildtype	wildtype
GCGS1095	0.5	Type II non-mosaic (NG STAR 2.002)	421P	R201H	wildtype
GCGS1014	0.125	Type II non-mosaic (NG STAR 2.002)	421P	wildtype	E98K
GCGS1013	0.125	Type II non-mosaic (NG STAR 2.002)	421P	wildtype	Δ92-95
GCGS0457 RpoB^{R201H}	0.25	Type II non-mosaic (NG STAR 2.002)	421P	R201H	wildtype
GCGS0457 RpoD^{E98K}	0.25	Type II non-mosaic (NG STAR 2.002)	421P	wildtype	E98K
GCGS0457 RpoD$^{\Delta 92\text{-}95}$	0.125	Type II non-mosaic (NG STAR 2.002)	421P	wildtype	Δ92-95
GCGS0364	0.023	Type II non-mosaic (NG STAR 2.002)	421P	wildtype	wildtype
GCGS0364 RpoB^{G158V}	0.5	Type II non-mosaic (NG STAR 2.002)	421P	G158V	wildtype
GCGS0364 RpoB^{P157L}	0.75	Type II non-mosaic (NG STAR 2.002)	421P	P157L	wildtype
GCGS0457 (pKH37)	≤0.016[a]	Type II non-mosaic (NG STAR 2.002)	421P	wildtype	wildtype
GCGS0457 (pKH37::*ponA*)	0.064[a]	Type II non-mosaic (NG STAR 2.002)	421P + inducible 421L	wildtype	wildtype
GCGS0457 (pKH37::*ponA*^{L421P})	0.064[a]	Type II non-mosaic (NG STAR 2.002)	421P + inducible 421P	wildtype	wildtype

[a]MIC measured in the presence of 0.5mM IPTG

bioRxiv preprint doi: https://doi.org/10.1101/626457; this version posted May 3, 2019. The copyright holder for this preprint (which was not certified by peer review) is the author/funder, who has granted bioRxiv a license to display the preprint in perpetuity. It is made available under aCC-BY-ND 4.0 International license.

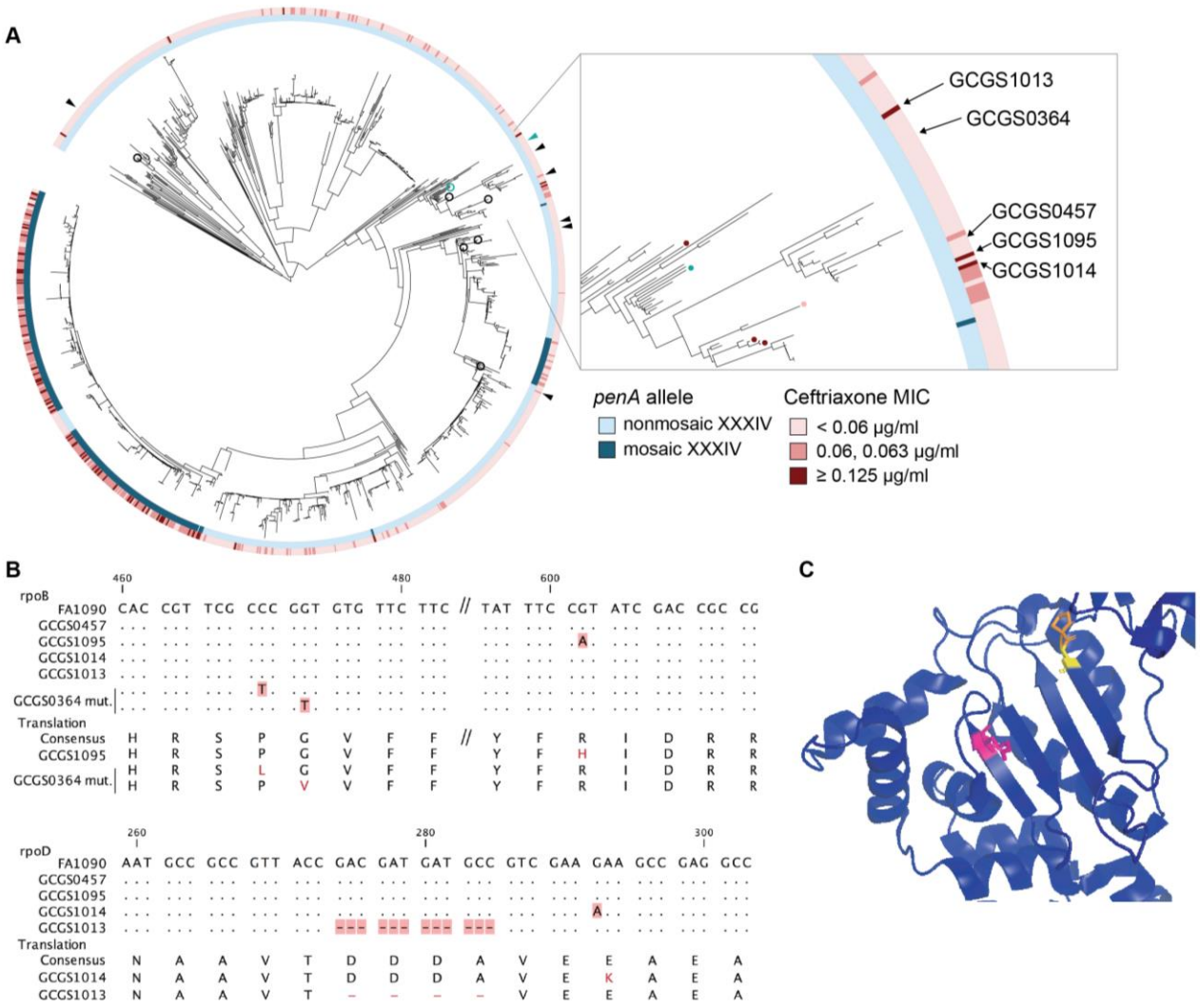

Figure 1. RNA polymerase-mediated reduced cephalosporin susceptibility among GISP isolates. (A) Most high-level reduced cephalosporin susceptibility (MIC ≥ 0.125 µg/mL) in the GISP dataset is associated with the mosaic *penA* XXXIV allele, but some isolates with high MICs lack this allele. Three of these isolates – GCGS1095, GCGS1014, and GCGS1013 (inset, red-marked branches) – have mutations in the RNA polymerase holoenzyme, which cause reduced cephalosporin susceptibility when transformed into susceptible clinical isolates (arrows and black-circled branches, left) such as the phylogenetic neighbor GCGS0457 (inset, pink-marked branch). The isolate GCGS0364 (teal) spontaneously develops CRO^{RS} via *rpoB* mutation *in vitro*. **(B)** Alignment of mutant RNA polymerase alleles associated with reduced ceftriaxone susceptibility. **(C)** Crystal structure of RpoB from *E. coli* by Zuo *et al.* (PDB 4YLO) [37], showing the location of the residues homologous to *N. gonorrhoeae* RpoB R201 (magenta), G158 (yellow), and P157 (orange).

bioRxiv preprint doi: https://doi.org/10.1101/626457; this version posted May 3, 2019. The copyright holder for this preprint (which was not certified by peer review) is the author/funder, who has granted bioRxiv a license to display the preprint in perpetuity. It is made available under aCC-BY-ND 4.0 International license.

A

Strain	MIC (μg/ml)							
	CRO	CFX	PEN	EPM	AZI	TET	CIP	RIF
GCGS0457	0.016	0.016	2	0.016	0.25	0.25	≤0.015	0.125
GCGS1095	0.5	1	2	0.032	0.5	1	≤0.015	≤0.0625
GCGS1014	0.125	0.5	1	0.032	0.25	1	≤0.015	≤0.0625
GCGS1013	0.125	0.5	0.5	0.023	0.5	2	≤0.015	≤0.0625
GCGS0457 RpoB^{R201H}	0.25	>0.5	1	0.047	0.25	0.25	≤0.015	≤0.0625
GCGS0457 RpoD^{E98K}	0.25	0.5	1	0.023	0.25	0.25	≤0.015	≤0.0625
GCGS0457 RpoD$^{\Delta 92\text{-}95}$	0.125	0.5	1	0.023	0.25	2	≤0.015	≤0.0625

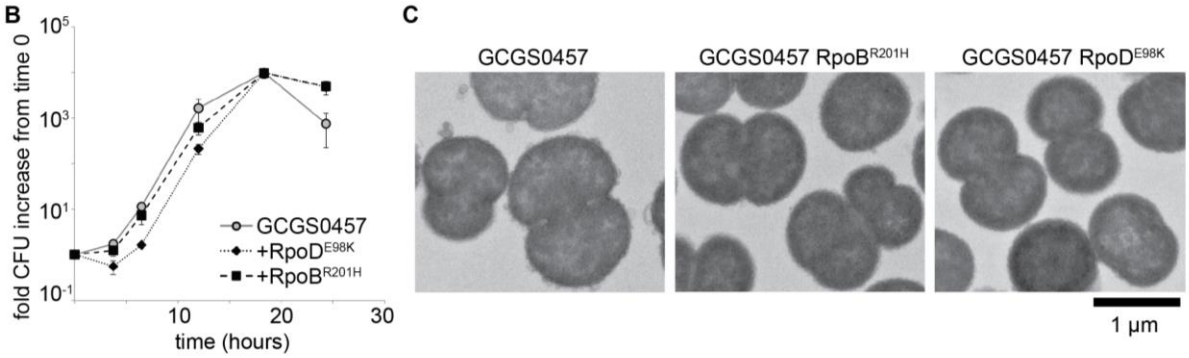

Figure 2. RNA polymerase mutations reduce susceptibility to cephalosporins, but do not alter susceptibility to other antimicrobial drugs, and do not change growth phenotypes. (**A**) Antimicrobial susceptibility profiles of parental isolates (GCGS0457, GCGS1095, GCGS1014, GCGS1013) and RNAP mutant transformants in the GCGS0457 background. The RNAP mutations found in parental CRO^{RS} isolates and in CRO^{RS} transformants decrease susceptibility to the cephalosporins ceftriaxone (CRO) and cefixime (CFX), but do not decrease susceptibility to benzylpenicillin (PEN), ertapenem (EPM), azithromycin (AZI), tetracycline (TET), ciprofloxacin (CIP), or rifampin (RIF). (**B**) Growth of GCGS0457 and RNAP mutant transformants on solid GCB agar (n=3, representative of two independent experiments). RNAP mutations do not result in a growth rate defect. (**C**) Transmission electron micrographs of GCGS0457 and RNAP mutant transformants. CRO^{RS} transformants are slightly smaller than the parental GCGS0457 strain, but are otherwise morphologically similar.

bioRxiv preprint doi: https://doi.org/10.1101/626457; this version posted May 3, 2019. The copyright holder for this preprint (which was not certified by peer review) is the author/funder, who has granted bioRxiv a license to display the preprint in perpetuity. It is made available under aCC-BY-ND 4.0 International license.

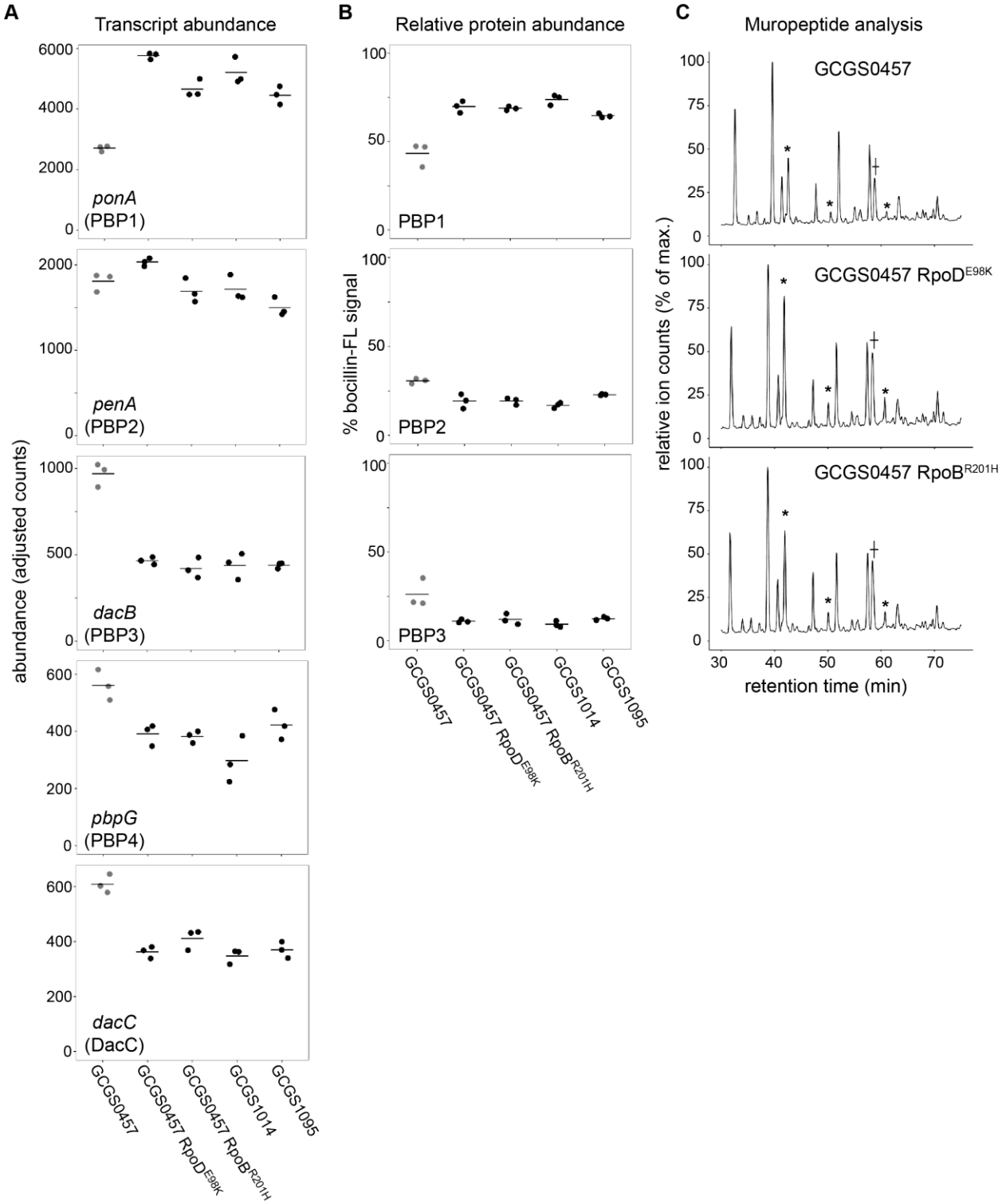

Figure 3. Effect of CRO^{RS}-associated RNAP mutations on PBP abundance and cell wall structure. (**A**) Normalized abundance of transcripts encoding penicillin binding proteins (PBPs) in parental isolates (GCGS0457, GCGS1095, GCGS1014) and RNAP mutant transformants in the GCGS0457 background, measured by RNAseq. (**B**) Relative protein abundance of PBP1,

bioRxiv preprint doi: https://doi.org/10.1101/626457; this version posted May 3, 2019. The copyright holder for this preprint (which was not certified by peer review) is the author/funder, who has granted bioRxiv a license to display the preprint in perpetuity. It is made available under aCC-BY-ND 4.0 International license.

PBP2, and PBP3, as measured by bocillin-FL labeling. Total bocillin-FL signal for each strain was set at 100%. The relative contribution of each PBP to that signal is shown here. PBP4 was not observed on these gels, in agreement with previous reports [38]. (**C**) Muropeptide analysis of GCGS0457 and RNAP mutant transformants. Transformant cell walls contain a higher proportion of peptidoglycan with pentapeptide stems (peaks marked with asterisks). † denotes a peak that includes two species: tetrapeptide monomer (-H_2O) and 4-3 crosslinked dimer between tetrapeptide and pentapeptide stems. Traces are representative of 2-3 independent experiments.

bioRxiv preprint doi: https://doi.org/10.1101/626457; this version posted May 3, 2019. The copyright holder for this preprint (which was not certified by peer review) is the author/funder, who has granted bioRxiv a license to display the preprint in perpetuity. It is made available under aCC-BY-ND 4.0 International license.

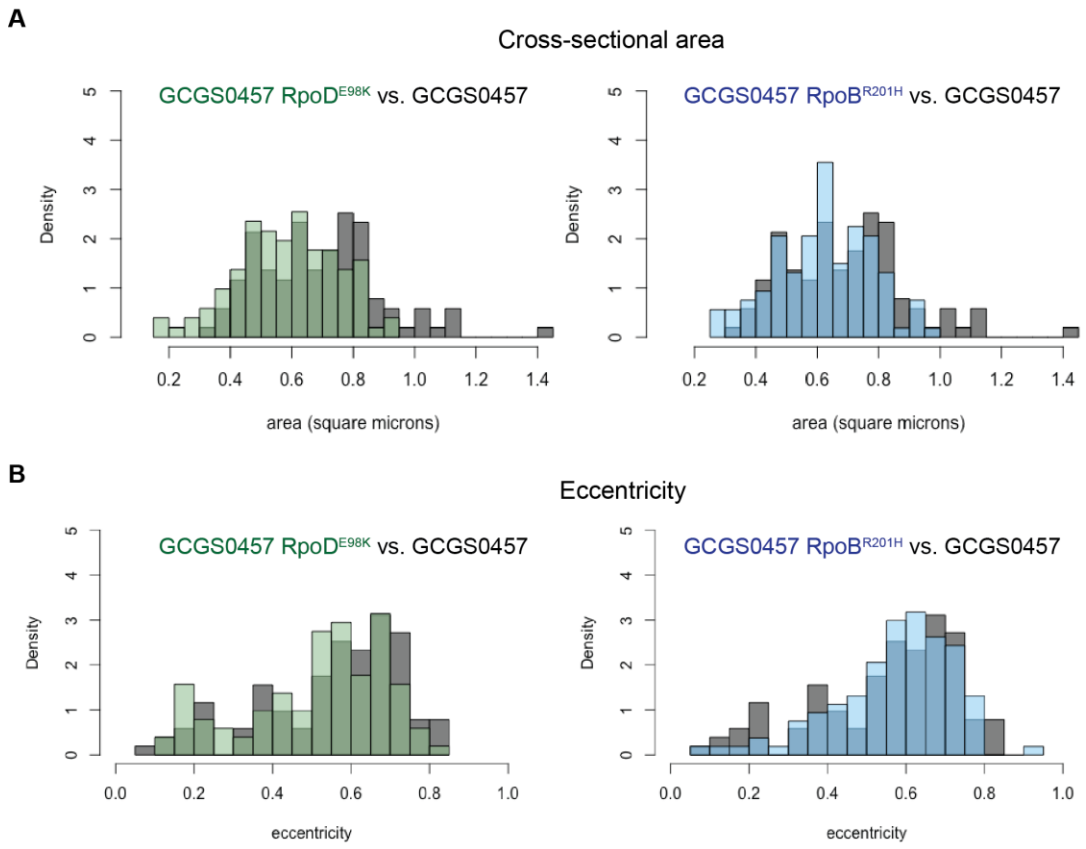

Supplementary Figure 1. Size and eccentricity of GCGS0457 and CRO^{RS} transformants. 100-105 cellular cross sections from TEM images were manually measured in ImageJ to measure the **(A)** cross-sectional area and **(B)** eccentricity of cells from the CRO^{S} strain GCGS0457 and its CRO^{RS} transformants GCGS0457 RpoD^{E98K} and GCGS0457 RpoB^{R201H}. The cross-sectional area of CRO^{RS} transformant cells is slightly smaller (mean area: 0.585 μm^2 for GCGS0457 RpoD^{E98K}; 0.621 μm^2 for GCGS0457 RpoB^{R201H}) than cells of the parental strain GCGS0457 (mean area 0.693 μm^2; $p = 3.977 \times 10^{-5}$ compared to GCGS0457 RpoD^{E98K} and p=0.00436 compared to GCGS0457 RpoB^{R201H} by Welch's t-test). The degree of eccentricity in the CRO cells is not significantly different between these populations.

bioRxiv preprint doi: https://doi.org/10.1101/626457; this version posted May 3, 2019. The copyright holder for this preprint (which was not certified by peer review) is the author/funder, who has granted bioRxiv a license to display the preprint in perpetuity. It is made available under aCC-BY-ND 4.0 International license.

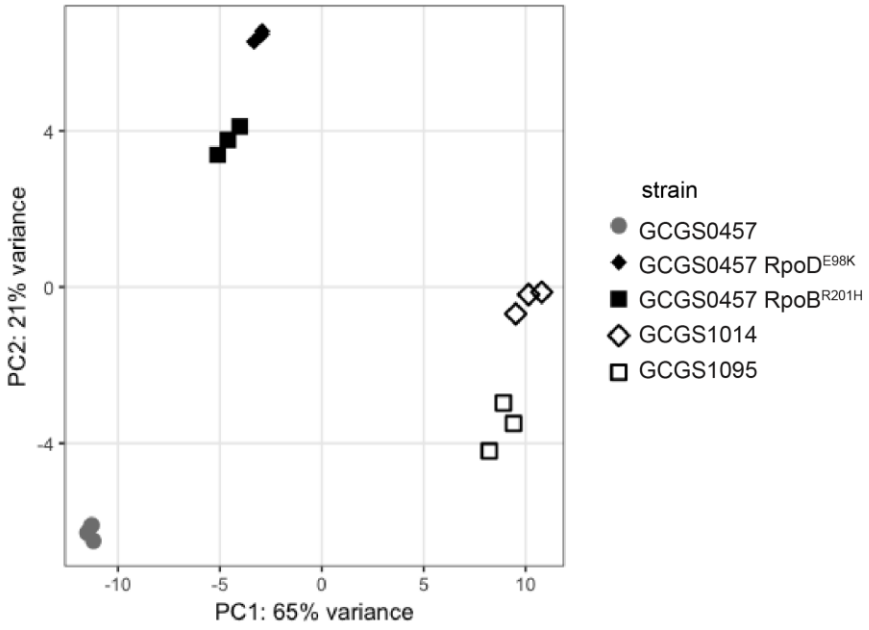

Supplementary Figure 2. Principle components analysis of RNA-seq data. The first two principle components are shown for transcriptomic data collected from the CRO^{S} isolate GCGS0457, the CRO^{RS} isolates GCGS1095 and GCGS1014, and the CRO^{RS} transformants GCGS0457 RpoD^{E98K} and GCGS0457 RpoB^{R201H} (three biological replicates/strain). Replicates from both CRO^{RS} transformants cluster tightly, despite having different RNAP mutations.

bioRxiv preprint doi: https://doi.org/10.1101/626457; this version posted May 3, 2019. The copyright holder for this preprint (which was not certified by peer review) is the author/funder, who has granted bioRxiv a license to display the preprint in perpetuity. It is made available under aCC-BY-ND 4.0 International license.

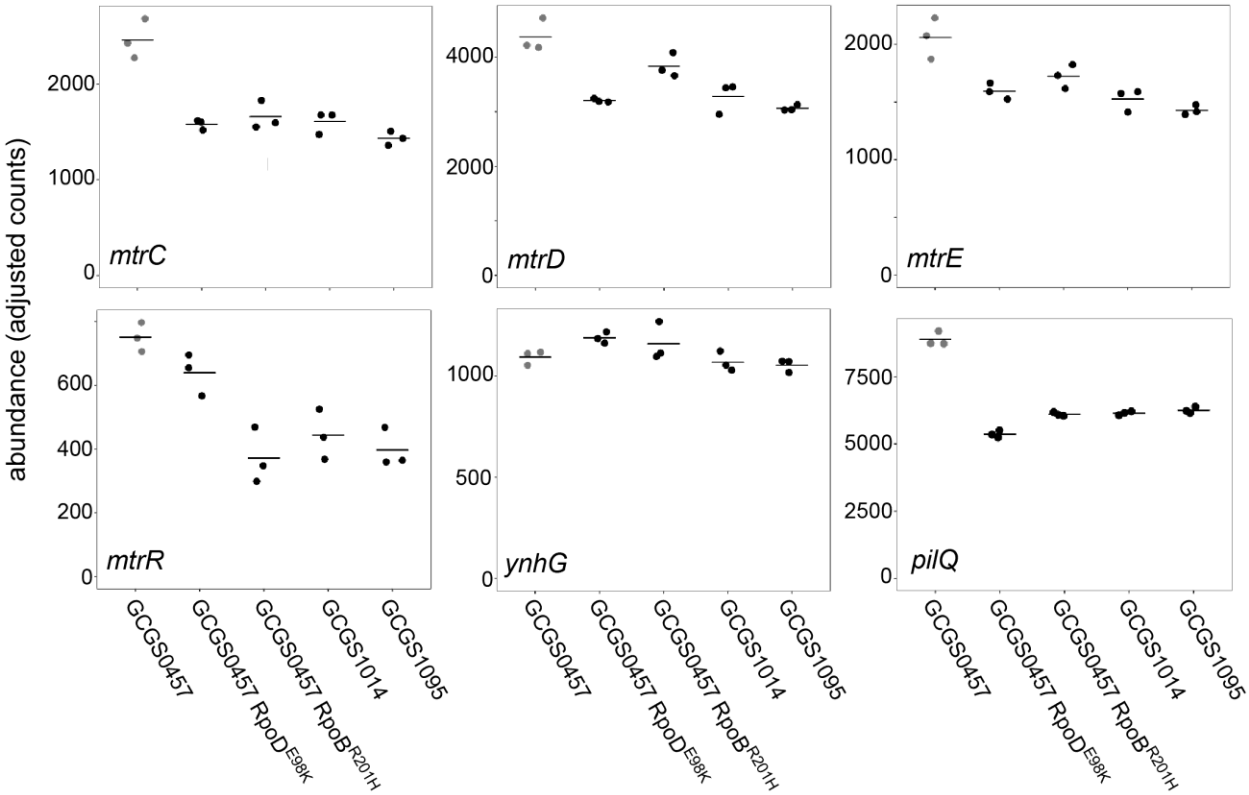

Supplementary Figure 3. Transcript abundance of various genes in CRO^{RS} strains with RNA polymerase mutations. Normalized abundance of various transcripts in parental isolates (GCGS0457, GCGS1095, GCGS1014) and RNAP mutant transformants in the GCGS0457 background. Shown: *mtrC*, *mtrD*, and *mtrE*, which encode the components of the Mtr efflux pump; *mtrR*, which encodes the transcriptional repressor of the *mtrCDE* operon; *ynhG*, a putative L,D-transpeptidase; and *pilQ*, which encodes the pilus pore subunit PilQ.

bioRxiv preprint doi: https://doi.org/10.1101/626457; this version posted May 3, 2019. The copyright holder for this preprint (which was not certified by peer review) is the author/funder, who has granted bioRxiv a license to display the preprint in perpetuity. It is made available under aCC-BY-ND 4.0 International license.

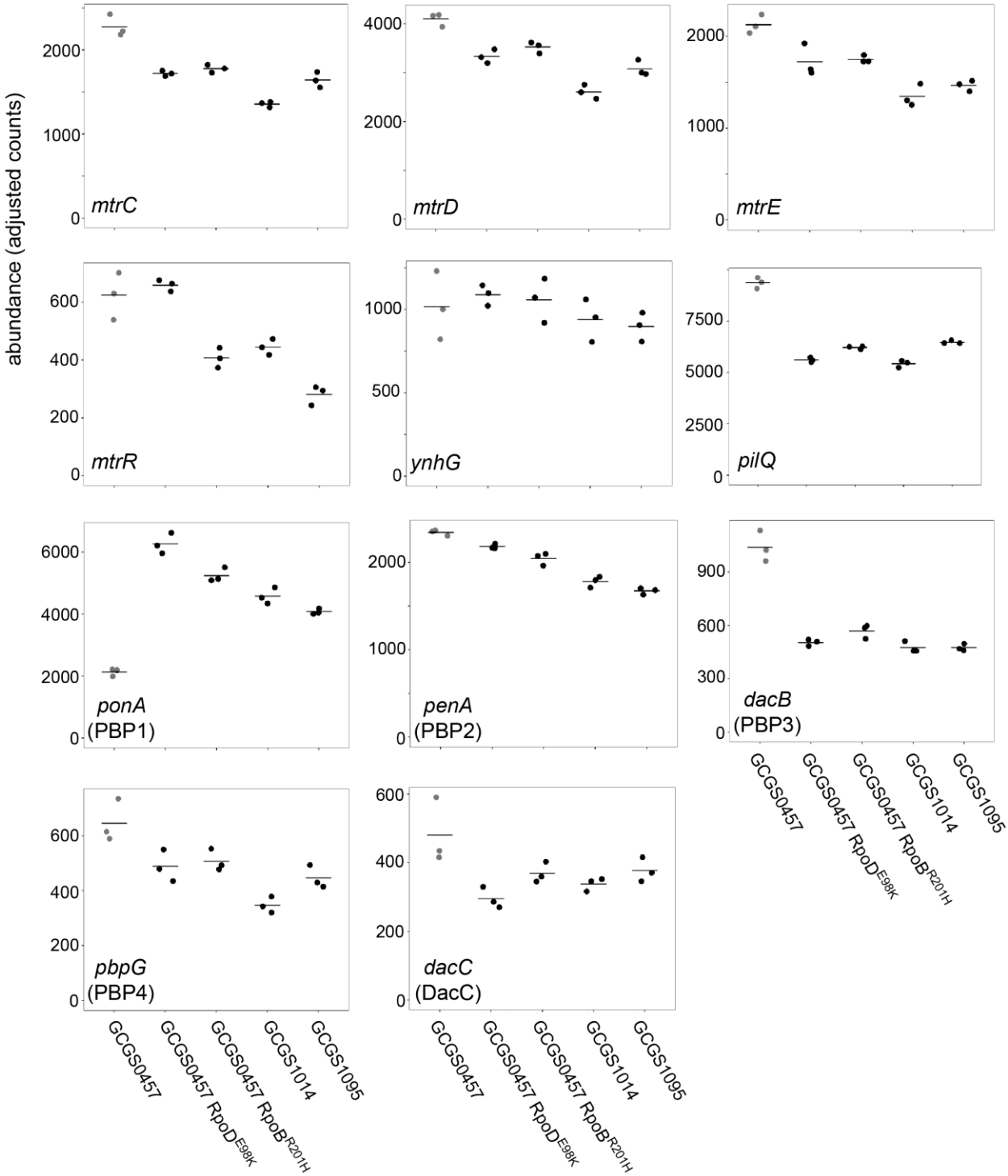

Supplementary Figure 4. Transcript abundance of various genes in CRO^{RS} strains with RNAP mutations, exposed to sub-inhibitory ceftriaxone. Normalized abundance of various transcripts in parental isolates (GCGS0457, GCGS1095, GCGS1014) and RNAP mutant transformants, exposed to 0.008 µg/mL CRO for 90 minutes. Shown: *mtrC*, *mtrD*, and *mtrE*, which encode the components of the Mtr efflux pump; *mtrR*, which encodes the transcriptional

bioRxiv preprint doi: https://doi.org/10.1101/626457; this version posted May 3, 2019. The copyright holder for this preprint (which was not certified by peer review) is the author/funder, who has granted bioRxiv a license to display the preprint in perpetuity. It is made available under aCC-BY-ND 4.0 International license.

repressor of the *mtrCDE* operon; *ynhG*, a putative L,D-transpeptidase; *pilQ*, which encodes the pilus pore subunit PilQ; and transcripts for each of the penicillin-binding proteins.

bioRxiv preprint doi: https://doi.org/10.1101/626457; this version posted May 3, 2019. The copyright holder for this preprint (which was not certified by peer review) is the author/funder, who has granted bioRxiv a license to display the preprint in perpetuity. It is made available under aCC-BY-ND 4.0 International license.

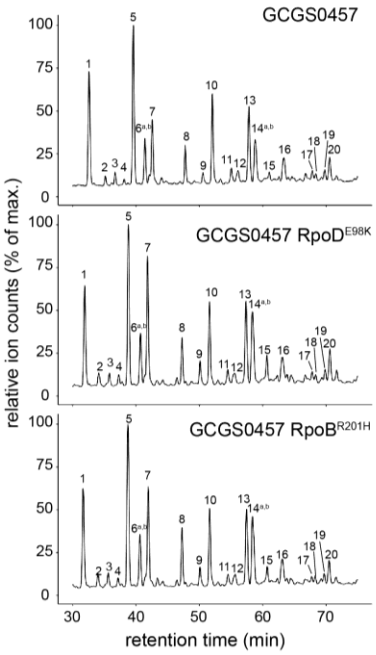

Peak	Proposed Structure	GCGS0457	GCGS0457 RpoD^{E98K}	GCGS0457 RpoB^{R201H}
1	Tripeptide	18.9	12.6	13.3
2	Tetrapeptide +Ala-mDAP	0.7	0.9	0.9
3	Peak 2 isomer	1.6	1.6	1.9
4	Pentapeptide (Gly)	0.4	0.9	0.8
5	Tetrapeptide	24.1	21.3	24.8
6a	Dipeptide	4.9	5.9	5.9
6b	Tripeptide (OAc)	2.8	1.9	2.1
7	Pentapeptide	8.1	15	12.2
8	Tetrapeptide (OAc)	4.3	4	5.4
9	Pentapeptide (OAc)	0.8	1.7	1.3
10	Tripeptide (–H_2O)	14.3	10.5	10.3
11	4-3 tetra-tri or 3-3 tri-tetra	0.8	0.6	0.4
12	Peak 11 isomer	0.6	0.5	0.5
13	4-3 tetra-tetra or 3-3 tri-penta	5.6	5	4.7
14a	Tetrapeptide (–H_2O)	4.6	6.7	7.8
14b	4-3 tetra-penta	1.6	2.6	1.9
15	Pentapeptide (–H_2O)	0.7	2.6	1.5
16	4-3 tetra-tetra or 3-3 tri-penta (OAc)	2	1.9	1.7
17	4-3 tetra-tri or 3-3 tri-tetra (–H_2O)	0.9	0.8	0.4
18	Peak 17 isomer	0.4	0.3	0.3
19	4-3 tetra-tetra or 3-3 tri-penta (–H_2O)	0.6	0.6	0.5
20	Peak 19 isomer	1.5	1.9	1.4
	Total Monomers	86.2	85.8	88.3
	Total Crosslinks	13.8	14.2	11.7

Supplementary Figure 5. Relative abundance of muropeptide peaks in cell wall digests of GCGS0457 and its CRO^{RS} derivatives, GCGS0457 RpoD^{E98K} and GCGS0457 RpoB^{R201H}. Data is representative of 2-3 independent experiments. Values were calculated by first extracting the peak mass from the total ion chromatogram, integrating the resulting peak area, and dividing by the sum of all of the peak areas within each sample. See Supplementary Table 2 for a listing of all muropeptide masses detected.

bioRxiv preprint doi: https://doi.org/10.1101/626457; this version posted May 3, 2019. The copyright holder for this preprint (which was not certified by peer review) is the author/funder, who has granted bioRxiv a license to display the preprint in perpetuity. It is made available under aCC-BY-ND 4.0 International license.

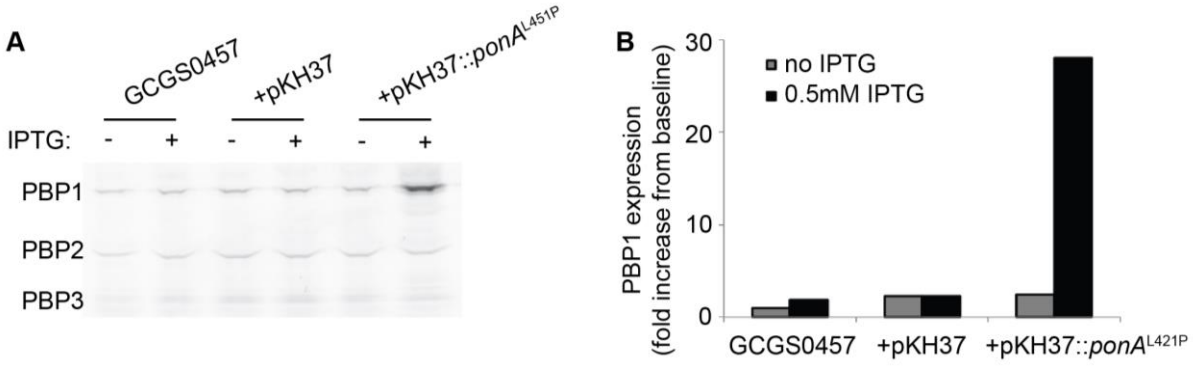

Supplementary Figure 6. Overexpression of PBP1. The CRO^{S} isolate GCGS0457 was transformed with the empty vector pKH37 or the PBP1 overexpression vector pKH37::*ponA*^{L421P}. Each strain was grown in the presence or absence of 0.5mM IPTG to induce the lac promoter on pKH37 and stained with bocillin-FL to fluorescently label PBPs. Proteins were separated by SDS-PAGE. **(A)** Image of bocillin-FL fluorescence in the SDS-PAGE gel, visualized with the Typhoon FLA-9500 system. **(B)** PBP1 expression was quantified by densitometry and normalized to PBP1 expression in GCGS0457 without IPTG. When induced with 0.5mM IPTG, the GCGS0457(pKH37::*ponA*^{L421P}) strain produces approximately 30-fold more PBP1.

bioRxiv preprint doi: https://doi.org/10.1101/626457; this version posted May 3, 2019. The copyright holder for this preprint (which was not certified by peer review) is the author/funder, who has granted bioRxiv a license to display the preprint in perpetuity. It is made available under aCC-BY-ND 4.0 International license.

Supplementary Table 1. Bacterial strains used in this study

***E. coli* strains**			
Strain name	**Description**	**Source**	**Strain number**
DH5α(pKH37::*ponA*)	Plasmid for inducible overexpression of wildtype *N. gonorrhoeae* PBP1	This study	YWP28
DH5α(pKH25::*ponA*^{L421P})	Plasmid for inducible overexpression of *N. gonorrhoeae* PBP1 with L421P substitution	This study	YWP04

***N. gonorrhoeae* strains**			
Strain name	**Description**	**Source**	**Strain number**
GCGS0457	CRO^{S} clinical isolate; recipient strain for transformations	GISP, CDC	
GCGS1013	CRO^{RS} clinical isolate	GISP, CDC	
GCGS1014	CRO^{RS} clinical isolate	GISP, CDC	
GCGS1095	CRO^{RS} clinical isolate	GISP, CDC	
28BL	CRO^{S} laboratory strain	Gift of S. Johnson	
FA1090	CRO^{S} laboratory strain	Gift of C. Genco	
SP300-SP311	12 independent CRO^{RS} transformants: GCGS0457 + gDNA from GCGS1014	This study	
SP312-SP314	3 independent CRO^{RS} transformants: GCGS0457 + gDNA from GCGS1095	This study	
GCGS0457 RpoD^{E98K}	Point mutation introduced on PCR product	This study	SP316
GCGS0457 RpoB^{R201H}	Point mutation introduced on PCR product	This study	SP319
GCGS0457 RpoD$^{\Delta 92\text{-}95}$	Deletion introduced on PCR product	This study	SP323
GCGS0092	CRO^{S} clinical isolate	GISP, CDC	
GCGS0092 RpoB^{R201H}	CRO^{RS} transformant; point mutation introduced on PCR product	This study	SP349
GCGS0275	CRO^{S} clinical isolate	GISP, CDC	
GCGS0275 RpoB^{R201H}	CRO^{RS} transformant; point mutation introduced on PCR product	This study	SP354
GCGS0465	CRO^{S} clinical isolate	GISP, CDC	
GCGS0465 RpoB^{R201H}	CRO^{RS} transformant; point mutation introduced on PCR product	This study	SP358
GCGS0336	CRO^{S} clinical isolate	GISP, CDC	
GCGS0336 RpoB^{R201H}	CRO^{RS} transformant; point mutation introduced on PCR product	This study	SP340
GCGS0524	CRO^{S} clinical isolate	GISP, CDC	
GCGS0524 RpoB^{R201H}	CRO^{RS} transformant; point mutation introduced on PCR product	This study	SP368
GCGS0364	CRO^{S} clinical isolate; develops spontaneous CRO^{RS} via *rpoB* mutation *in vitro*	GISP, CDC	
GCGS0364 RpoB^{G158V}	Point mutation introduced on PCR product	This study	SP377
GCGS0364 RpoB^{P157L}	Point mutation introduced on PCR product	This study	SP375
GCGS0457		This study	YWE12

bioRxiv preprint doi: https://doi.org/10.1101/626457; this version posted May 3, 2019. The copyright holder for this preprint (which was not certified by peer review) is the author/funder, who has granted bioRxiv a license to display the preprint in perpetuity. It is made available under aCC-BY-ND 4.0 International license.

(pKH37)			
GCGS0457 (pKH37::*ponA*)	Inducible overexpression of PBP1	This study	YWB02
GCGS0457 (pKH37::*ponA*^{L421P})	Inducible overexpression of the PBP1^{L421P} variant	This study	YWC02

bioRxiv preprint doi: https://doi.org/10.1101/626457; this version posted May 3, 2019. The copyright holder for this preprint (which was not certified by peer review) is the author/funder, who has granted bioRxiv a license to display the preprint in perpetuity. It is made available under aCC-BY-ND 4.0 International license.

Supplementary Table 2. Muropeptide masses detected in cell wall digests of GCGS0457 and RNAP mutants.

Peak	Proposed Structure[a]	Theoretical Mass (charge)	Observed Mass (charge)
1	Tripeptide	871.3779 (1), 436.1926 (2)	871.3783 (1), 436.1925 (2)
2	Tetrapeptide +Ala-mDAP[2]	1185.5369 (1), 593.2721 (2)	593.2719 (2)
3	Peak 2 isomer	1185.5369 (1), 593.2721 (2)	593.2721 (2)
4	Pentapeptide (Gly)	999.4364 (1), 500.2219 (2)	999.4360 (1), 500.2213 (2)
5	Tetrapeptide	942.4150 (1), 471.7111 (2)	942.4151 (1), 471.7109 (2)
6a	Dipeptide	699.2931 (1), 721.275 (1+Na)	699.2937 (1), 721.2754 (1+Na)
6b	Tripeptide (OAc)	913.3884 (1), 457.1979 (2)	913.3893 (1), 457.1974
7	Pentapeptide	1013.4521 (1), 507.2297 (2)	1013.4527 (1), 507.2297 (2)
8	Tetrapeptide (OAc)	984.4255 (1), 492.7164 (2)	984.4264 (1), 492.7163 (2)
9	Pentapeptide (OAc)	1055.4627 (1), 528.235 (2)	1055.4684 (1), 528.2345 (2)
10	Tripeptide (–H_2O)	851.3517 (1), 426.1795 (2)	851.3520 (1)
11	4-3 tetra-tri or 3-3 tri-tetra[c]	897.8911 (2), 598.9299 (3)	897.8924 (2), 598.9295 (3)
12	Peak 11 isomer	897.8911 (2), 598.9299 (3)	897.8924 (2), 598.9295 (3)
13	4-3 tetra-tetra or 3-3 tri-penta[c]	933.4097 (2), 622.6089 (3)	933.4117 (2), 622.6091 (3)
14a	Tetrapeptide (–H_2O)	922.3888 (1), 461.698 (2)	922.3906 (1), 461.6981 (2)
14b	4-3 tetra-penta	968.9283 (2), 646.2879 (3)	968.9309 (2), 646.2888 (3)
15	Pentapeptide (–H_2O)	993.4259 (1), 497.2166 (2)	933.4257 (1), 497.2163 (2)
16	4-3 tetra-tetra or 3-3 tri-penta (OAc)[c]	954.4150 (2), 636.6124 (3)	954.4165 (2), 636.6124 (2)
17	4-3 tetra-tri or 3-3 tri-tetra (–H_2O)[c]	887.878 (2), 592.2544 (3)	887.8792 (2), 592.2543 (3)
18	Peak 17 isomer	887.878 (2), 592.2544 (3)	887.8792 (2), 592.2543 (3)
19	4-3 tetra-tetra or 3-3 tri-penta (–H_2O)[c]	923.3966 (2), 615.9335 (3)	923.3977 (2), 615.9332 (3)
20	Peak 19 isomer	923.3966 (2), 615.9335 (3)	923.3977 (2), 615.9332 (3)

[a] The pentapeptide stem in *N. gonorrhoeae* is L-Ala-γ-D-Glu-L-mDap-D-Ala-D-Ala. OAc = O-acetylation of MurNAc. –H_2O = 1,6-anhdro-MurNAc. Gly = replacement of one D-Ala residue with glycine.

[b] This structure is the product of cleavage of a 4-3 crosslink.

[c] Mass is consistent with either a 4-3 (PBP-mediated) crosslink or a 3-3 (L,D-transpeptidase-mediated) crosslink.

Supplementary File 1 (Excel workbook). Allelic diversity of RNA polymerase holoenzyme components and sigma factors.

bioRxiv preprint doi: https://doi.org/10.1101/626457; this version posted May 3, 2019. The copyright holder for this preprint (which was not certified by peer review) is the author/funder, who has granted bioRxiv a license to display the preprint in perpetuity. It is made available under aCC-BY-ND 4.0 International license.

References

1 Centers for Disease Control and Prevention. *Gonorrhea -- Sexually Transmitted Disease Surveillance 2017*, <https://http://www.cdc.gov/std/stats17/gonorrhea.htm> (2018).

2 Kirkcaldy, R. D. *et al.* Neisseria gonorrhoeae Antimicrobial Susceptibility Surveillance — The Gonococcal Isolate Surveillance Project, 27 Sites, United States, 2014. *MMWR. Surveillance Summaries* **65**, 1-19, doi:10.15585/mmwr.ss6507a1 (2016).

3 Demczuk, W. *et al.* Whole-genome phylogenomic heterogeneity of Neisseria gonorrhoeae isolates with decreased cephalosporin susceptibility collected in Canada between 1989 and 2013. *Journal of Clinical Microbiology* **53**, 191-200, doi:10.1128/JCM.02589-14 (2015).

4 Eyre, D. W. *et al.* Gonorrhoea treatment failure caused by a Neisseria gonorrhoeae strain with combined ceftriaxone and high- level azithromycin resistance, England, February 2018. *Eurosurveillance* **23**, 1800323, doi:10.2807/1560-7917.ES.2018.23.27.1800323 (2018).

5 Public Health England. Surveillance of antimicrobial resistance in Neisseria gonorrhoeae in England and Wales. Key findings from the Gonococcal Resistance to Antimicrobials Surveillance Programme (GRASP). Anti-microbial resistance in Neisseria gonorrhoeae: data to May 2018. 1-25 (Public Health England, London, United Kingdom, 2018).

6 Fifer, H., Saunders, J., Soni, S., Sadiq, S. T. & FitzGerald, M. British Association for Sexual Health and HIV national guideline for the management of infection with Neisseria gonorrhoeae (2019). 1-25 (2019).

7 Eyre, D. W. *et al.* Detection in the United Kingdom of the Neisseria gonorrhoeae FC428 clone, with ceftriaxone resistance and intermediate resistance to azithromycin, October to December 2018. *Eurosurveillance* **24**, doi:10.2807/1560-7917.ES.2019.24.10.1900147 (2019).

8 Zhao, S. *et al.* Genetics of chromosomally mediated intermediate resistance to ceftriaxone and cefixime in Neisseria gonorrhoeae. *Antimicrobial agents and chemotherapy* **53**, 3744-3751, doi:10.1128/AAC.00304-09 (2009).

9 Lindberg, R., Fredlund, H., Nicholas, R. & Unemo, M. Neisseria gonorrhoeae isolates with reduced susceptibility to cefixime and ceftriaxone: Association with genetic polymorphisms in penA, mtrR, porB1b, and ponA. *Antimicrobial agents and chemotherapy* **51**, 2117-2122, doi:10.1128/AAC.01604-06 (2007).

10 Whiley, D. M. *et al.* Reduced susceptibility to ceftriaxone in Neisseria gonorrhoeae is associated with mutations G542S, P551S and P551L in the gonococcal penicillin-binding protein 2. *Journal of Antimicrobial Chemotherapy* **65**, 1615-1618, doi:10.1093/jac/dkq187 (2010).

11 Kocaoglu, O. & Carlson, E. E. Profiling of β-lactam selectivity for penicillin-binding proteins in Escherichia coli strain DC2. *Antimicrobial agents and chemotherapy* **59**, 2785-2790, doi:10.1128/AAC.04552-14 (2015).

12 Grad, Y. H. *et al.* Genomic epidemiology of gonococcal resistance to extended-spectrum cephalosporins, macrolides, and fluoroquinolones in the United States, 2000-2013. *J Infect Dis* **214**, 1579-1587, doi:10.1093/infdis/jiw420 (2016).

13 Peng, J.-P. *et al.* A Whole-genome Sequencing Analysis of Neisseria gonorrhoeae Isolates in China: An Observational Study. *EClinicalMedicine* **7**, 47-54, doi:10.1016/j.eclinm.2019.01.010 (2019).

bioRxiv preprint doi: https://doi.org/10.1101/626457; this version posted May 3, 2019. The copyright holder for this preprint (which was not certified by peer review) is the author/funder, who has granted bioRxiv a license to display the preprint in perpetuity. It is made available under aCC-BY-ND 4.0 International license.

14 Abrams, A. J. *et al.* A Case of Decreased Susceptibility to Ceftriaxone in Neisseria gonorrhoeae in the Absence of a Mosaic Penicillin-Binding Protein 2 (penA) Allele. *Sexually Transmitted Diseases* **44**, 492-494, doi:10.1097/OLQ.0000000000000645 (2017).

15 Whiley, D. M., Limnios, E. A., Ray, S., Sloots, T. P. & Tapsall, J. W. Diversity of penA alterations and subtypes in Neisseria gonorrhoeae strains from Sydney, Australia, that are less susceptible to ceftriaxone. *Antimicrobial agents and chemotherapy* **51**, 3111-3116, doi:10.1128/AAC.00306-07 (2007).

16 Wadsworth, C., Sater, M. R., Bhattacharyya, R. P. & Grad, Y. H. Impact of population structure in the design of RNA-based diagnostics for antibiotic resistance in Neisseria gonorrhoeae. *bioRxiv*, 1-39, doi:http://dx.doi.org/10.1101/537175 (2019).

17 Sauvage, E., Kerff, F., Terrak, M., Ayala, J. A. & Charlier, P. The penicillin-binding proteins: Structure and role in peptidoglycan biosynthesis. *FEMS Microbiology Reviews* **32**, 234-258, doi:10.1111/j.1574-6976.2008.00105.x (2008).

18 Obergfell, K. P., Schaub, R. E., Priniski, L. L., Dillard, J. P. & Seifert, H. S. The low-molecular-mass, penicillin-binding proteins DacB and DacC combine to modify peptidoglycan cross-linking and allow stable Type IV pilus expression in Neisseria gonorrhoeae. *Molecular Microbiology* **109**, 135-149, doi:10.1111/mmi.13955 (2018).

19 Kohler, P. L., Hamilton, H. L., Cloud-Hansen, K. & Dillard, J. P. AtlA functions as a peptidoglycan lytic transglycosylase in the Neisseria gonorrhoeae type IV secretion system. *Journal of Bacteriology* **189**, 5421-5428, doi:10.1128/JB.00531-07 (2007).

20 Ropp, P. A., Hu, M., Olesky, M. & Nicholas, R. A. Mutations in ponA, the gene encoding penicillin-binding protein 1, and a novel locus, penC, are required for high-level chromosomally mediated penicillin resistance in Neisseria gonorrhoeae. *Antimicrobial agents and chemotherapy* **46**, 769-777, doi:10.1128/AAC.46.3.769-777.2002 (2002).

21 Zhao, S., Tobiason, D. M., Hu, M., Seifert, H. S. & Nicholas, R. A. The penC mutation conferring antibiotic resistance in Neisseria gonorrhoeae arises from a mutation in the PilQ secretin that interferes with multimer stability. *Molecular Microbiology* **57**, 1238-1251, doi:10.1111/j.1365-2958.2005.04752.x (2005).

22 Johnson, S. R. *et al.* In vitro selection of Neisseria gonorrhoeae mutants with elevated MIC values and increased resistance to cephalosporins. *Antimicrobial agents and chemotherapy* **58**, 6986-6989, doi:10.1128/AAC.03082-14 (2014).

23 Kellogg, D. S., Peacock, W. L., Deacon, W. E., Brown, L. & Pirkle, C. I. Neisseria gonorrhoeae: Virulence genetically linked to clonal variation. *Journal of Bacteriology* **85**, 1274-1279 (1963).

24 Rudel, T., van Putten, J. P. M., Gibbs, C. P., Haas, R. & Meyer, T. F. Interaction of two variable proteins (PilE and PilC) required for pilus-mediated adherence of Neisseria gonorrhoeae to human epithelial cells. *Molecular Microbiology* **6**, 3439-3450, doi:10.1111/j.1365-2958.1992.tb02211.x (1992).

25 Morse, S. A., Johnson, S. R., Biddle, J. W. & Roberts, M. C. High-level tetracycline resistance in Neisseria gonorrhoeae is result of acquisition of streptococcal tetM determinant. *Antimicrobial agents and chemotherapy* **30**, 664-670, doi:10.1128/AAC.30.5.664 (1986).

26 Wadsworth, C. B., Arnold, B. J., Abdul Sater, M. R. & Grad, Y. H. Azithromycin Resistance through Interspecific Acquisition of an Epistasis-Dependent Efflux Pump

bioRxiv preprint doi: https://doi.org/10.1101/626457; this version posted May 3, 2019. The copyright holder for this preprint (which was not certified by peer review) is the author/funder, who has granted bioRxiv a license to display the preprint in perpetuity. It is made available under aCC-BY-ND 4.0 International license.

Component and Transcriptional Regulator in Neisseria gonorrhoeae. *mBio* **9**, e01419-01418 (2018).

27 Ambur, O. H., Frye, S. A. & Tønjum, T. New functional identity for the DNA uptake sequence in transformation and its presence in transcriptional terminators. *Journal of Bacteriology* **189**, 2077-2085, doi:10.1128/JB.01408-06 (2007).

28 Kim, S. *et al.* High-throughput automated microfluidic sample preparation for accurate microbial genomics. *Nature communications* **8**, 13919, doi:10.1038/ncomms13919 (2017).

29 Li, H. & Durbin, R. Fast and accurate long-read alignment with Burrows-Wheeler transform. *Bioinformatics* **26**, 589-595, doi:10.1093/bioinformatics/btp698 (2010).

30 Walker, B. J. *et al.* Pilon: An integrated tool for comprehensive microbial variant detection and genome assembly improvement. *PLoS ONE* **9**, doi:10.1371/journal.pone.0112963 (2014).

31 Rudy, R. F. *et al.* Simultaneous generation of many RNA-seq libraries in a single reaction. *Nature Methods* **12**, 323-325, doi:10.1038/nmeth.3313 (2015).

32 Zhu, Y. Y., Machleder, E. M., Chenchik, A., Li, R. & Siebert, P. D. Reverse transcriptase template switching: A SMART™ approach for full-length cDNA library construction. *BioTechniques* **30**, 892-897, doi:10.2144/01304pf02 (2001).

33 Love, M. I., Huber, W. & Anders, S. Moderated estimation of fold change and dispersion for RNA-seq data with DESeq2. *Genome Biology* **15**, 1-21, doi:10.1186/s13059-014-0550-8 (2014).

34 Schneider, C. A., Rasband, W. S. & Eliceiri, K. W. NIH Image to ImageJ: 25 years of image analysis. *Nature Methods* **9**, 671-675, doi:10.1038/nmeth.2089 (2012).

35 Kühner, D., Stahl, M., Demircioglu, D. D. & Bertsche, U. From cells to muropeptide structures in 24 h: Peptidoglycan mapping by UPLC-MS. *Scientific Reports* **4**, 7494, doi:10.1038/srep07494 (2014).

36 Gunn, J. S. & Stein, D. C. Use of a non-selective transformation technique to construct a multiply restriction/modification deficient mutant of Neisseria gonorrhoeae. *Molecular and General Genetics* **251**, 509-517, doi:10.1007/s004380050196 (1996).

37 Zuo, Y. & Steitz, T. A. Crystal structures of the e.coli transcription initiation complexes with a complete bubble. *Molecular Cell* **58**, 534-540, doi:10.1016/j.molcel.2015.03.010 (2015).

38 Zapun, A., Morlot, C. & Taha, M.-K. Resistance to β-Lactams in Neisseria ssp Due to Chromosomally Encoded Penicillin-Binding Proteins. *Antibiotics* **5**, 35, doi:10.3390/antibiotics5040035 (2016).